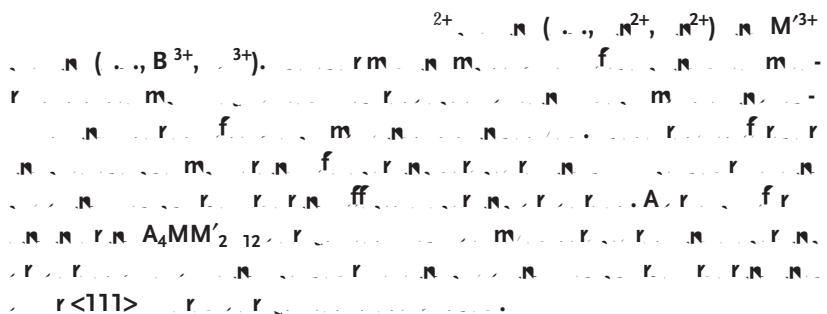


Double Perovskite $A_2M_2X_6$ with ABX_3 and AMX_3 Layers

Zhen Li, Xingang Zhao, Alex Zunger,* and Lijun Zhang*



1. Introduction

Halide perovskites with general formula AMX_3 (A is monovalent alkali or organic cation, M is divalent group IV metalloid Pb^{2+} or Sn^{2+} , and X represents halide anion Cl^- , Br^- , or I^-) have attracted enormous attention for various optoelectronic applications over the last few years owing to their flexibly tunable bandgap, high efficient photoluminescence yield, narrow

the recorded photovoltaic (PV) efficiency is over 23% in the laboratory.^[1,4-6] Such merits for high-performance optoelectronics are governed by their unique electronic structure features, which can mainly be attributed to the ns^2 lone-pair electrons of Pb^{2+} and Sn^{2+} cations.^[7,8] The presence of ns^2

bonding hybridization with the halide anions. This facilitates the formation of the shallow defect states to induce carriers, balanced and low electron and hole effective masses for efficient charge transport and carrier extraction.

Additionally, the enhanced Born effective charges (relative to nominal ionic charges) and large static dielectric constant contribute to screening charged defects and impurities, thereby suppressing carrier scattering and trapping.^[7,10] Despite the progress achieved in halide perovskites for optoelectronic applications, the poor long-term material and device stability under normal operation condition impedes their commercialization,^[4,11,12] though protecting active perovskite layers,^[4,6,9] mixing organic and inorganic A site ions,^[13,14] and exploiting low-dimensional counterparts have shown enhanced stability.^[14-16] More importantly, at this stage it is not clear whether the toxic issue of Pb^{2+} ions would hinder the practical device application of halide perovskites.

In this regard, eco-friendly Bi^{3+} - and Sb^{3+} -based perovskites with the similar ns^2 electron configuration as Pb^{2+} have attracted significant research interest.^[17-19] Within the three-dimensional (3D) perovskite framework formed by corner-sharing octahedral motifs, lead-free double halide perovskites have been proposed by hetero-substituting Pb^{2+} with the cation pair of monovalent metal (e.g., Na^+ , Ag^+) and trivalent metal (e.g., Sb^{3+} , Bi^{3+} , and In^{3+}) by exploiting the cation transmutation principle in conventional tetrahedral semiconductors.^[20-23] It is worth noting that the predicted inorganic double perovskites, such as $Cs_2AgBiCl_6$, $Cs_2AgBiBr_6$, $Cs_2AgInCl_6$, have been experimentally proved more stable against decomposition under humidity and light emission.^[21,22,24] However, these quaternary double perovskites exhibit weak light emission/absorption because of the indirect bandgap feature or the parity-forbidden

Dr. Z. Li, Dr. X. Zhao, Prof. L. Zhang
 State Key Laboratory of Superhard Materials
 Key Laboratory of Automobile Materials of MOE
 and School of Materials Science and Engineering
 Jilin University
 Changchun 130012, China
 E-mail: lijun_zhang@jlu.edu.cn
 Dr. X. Zhao, Prof. A. Zunger
 University of Colorado and Renewable and Sustainable Energy Institute
 Boulder, Colorado 80309, USA
 E-mail: Alex.Zunger@colorado.edu

The ORCID identification number(s) for the author(s) of this article can be found under <https://doi.org/10.1002/aelm.201900234>.

the charge neutrality condition constrains the ability to form a 3D corner-sharing perovskites structure.^[17,18,26] Instead, it forms compounds with 0D isolated dimer structure (with face-fused bi-octahedron) or 2D layered structure (with corner-sharing octahedron).^[17,18,26,27] Generally, the low-dimensional derived M^{3+} halide makes a framework with the unit formula of $A_{n+1}M_nX_{3n+3}$ being stabilized by stoichiometric cationic sublat-

parent ABX_3 perovskites.^[35] However, it involves more complexity due to the layered charge order and its discontinuity along the [111] direction. In comparison with the tilting equivalents in the parent cubic symmetry groups, the B-site cation order along the [111] direction makes the R_4^+ octahedral tilting to distinguishing between a positive ($a^-a^-c^0$) and a negative rotation ($-a^-a^-c^0$) along the [110] direction.^[35] These different type of distortion correlates with the redistribution of the ion charge and bonding angles, which affect the electronic properties and structural stability.^[33,36-38] Thus, the mixed-cation in the layered perovskite provides a living example to explore the coupling between the structural charge order and the octahedral tilting preferences in $A_4MM'_2X_{12}$ structure prototype.

Here we take a systematic screening procedure to explore the stability and optoelectronic property of the candidate $A_4MM'_2X_{12}$ compounds. Based on the above discussion, the Sn^{2+} and Zn^{2+} are intuitively the preferable cations due to their nearby element position with Sb^{3+} and Cu^{2+} in the periodic table, respectively. We, thus, extend precise screening steps and filters to study the possible ion combinations in $A_4MM'_2X_{12}$ halide compound with different cations for A = (K^+ and Cs^+), M = (Zn^{2+} and Sn^{2+}), M' = (Bi^{3+} and Sb^{3+}), and three types of ions for X =

relative energy in the other 5 Sn–Sb exchanged configuration (D1–D5) is at least 0.07 eV f.u.⁻¹ higher than the reference structure (OC). Thus, we choose the tri-layered cation ordered perovskite as the tentative structure for $A_4MM'_2X_{12}$. After the structure optimization, we find that all of the K-based perovskites only adopt octahedral tilting configurations ($a^-b^0c^0$ in Glazer's notation) while the Cs-based structures can adopt both original flat ($a^0b^0c^0$) and slightly tilting ($a^-b^0c^0$) structures. The total energies in those tilting configurations are lower energy than the flat layered structures. Thus, we take the tilting octahedron ($a^-b^0c^0$) configuration in further thermodynamic stability analysis.

3.1.2. Thermodynamic Stability Analysis

After establishing the ground-state structure for the compounds in step A, we next enquire which decorations are stable with respect to the decomposition to competing phases. For efficient screening of stable materials, we have used the two filters in step B. In step B.1, we considered 3 simplified decomposition pathways, then in step B.2, we considered all possible competing pathways through triangle analysis.

B.1 Simplified Decomposition Trends for the Thermodynamic Stability: In step B.1, we have considered three decomposition pathways:

- Decompose into binaries halides: $A_4MM'_2X_{12} \rightarrow 4AX + MX_2 + 2M'X_3$ (red bars);
- Decompose into binaries and ternary dimer $A_3M'_2X_9$: $A_4MM'_2X_{12} \rightarrow AX + MX_2 + A_3M'_2X_9$ (blue bars);
- Decompose into binaries and ternary layered $A_3M'_2X_9$: $A_4MM'_2X_{12} \rightarrow AX + MX_2 + A_3M'_2X_9$ -L (green bars).

The comparisons of decomposition pathways can give a quantitative stability tendency for the $A_4MM'_2X_{12}$

$\text{Cs}_4\text{ZnBi}_2\text{Cl}_{12}$, $\text{Cs}_4\text{ZnBi}_2\text{Br}_{12}$, and $\text{Cs}_4\text{ZnBi}_2\text{I}_{12}$. These compounds can be excluded because they are unstable against the $\text{A}_3\text{M}'_2\text{X}_9$ phase compounds.

The tendency of the enthalpies in Figure 2 shows that the stability for all combinations are decreasing when the halide ions

functional predicated bandgaps are even more close to the real values. Typically, the standard PBE functional severely underestimates the bandgaps for most wide bandgap semiconductors due to its unphysical self-Coulomb repulsion.^[51] However, the spin-orbit coupling has a strong effect on the lead halide perovskites, reducing the bandgap by up to roughly 1.0 eV; thus these two effects have canceled each other in the standard PBE predictions.^[3,52] For the heavier homologous element, Bi, with its more relatively contracted s-like states, we expect similar bandgap reduction; thus, the PBE functional would give a closer prediction. While the SOC effect on other Sn- and Sb-based perovskites was found to be weaker. As discussed in the Computational Methods section, the 2D layered $\text{Rb}_3\text{Sb}_2\text{Br}_9$ has measured gap of 2.48 eV and the PBE calculated bandgap of 1.76 eV, while HSE06 functional gives a closer prediction (2.35 eV), which implies a reliable method in the community. To get accurate bandgap prediction for the new compounds, we take the hybrid functional to correct the bandgap obtained by using PBE function with the SOC effects. The results are illustrated in Table 1 and **Figure 3**. All 6 compounds have quasi-direct band edge transition from valence band maxima (VBM) at Z point to the conduction band minima (CBM) at G point because the energy difference between the direct and indirect bandgaps in these compounds is very small (0.02–0.12 eV). Therefore, the direct bandgap transitions for those compounds

are within the range of visible light region (2.1–2.7 eV). From Figure 3 and Table 1, we can clearly see that the gap values increase with reducing the cation size from $A = \text{Rb}^+$ to K^+ for $\text{A}_4\text{SnM}'_2\text{X}_{12}$. For example, $\text{Rb}_4\text{SnBi}_2\text{Cl}_{12}$ and $\text{Rb}_4\text{SnSb}_2\text{Br}_{12}$ with bandgaps of 1.86 and 1.57 eV have increased to 1.92 and 1.64 eV as for $\text{K}_4\text{SnBi}_2\text{Cl}_{12}$ and $\text{K}_4\text{SnSb}_2\text{Br}_{12}$, respectively. This is because the smaller K^+ cation induces larger bond angle distortions in the $[\text{SnX}_6]^{4-}$ octahedrons, which destabilizes the antibonding from X(s/p) hybridization with the Sn(5p) orbitals while stabilizes it with the Sn-s orbitals. Thus it elevates the conduction band edges and reduces the valence band edges.^[53,54] A similar chemical trend was observed in the halide ions, i.e., from Br^- to Cl^- , the bandgap increased from 1.57 eV in $\text{Rb}_4\text{SnSb}_2\text{Br}_{12}$ to 1.64 eV in $\text{Rb}_4\text{SnSb}_2\text{Cl}_{12}$. This bandgap reduction can be understood on the basis of decreasing the

masses of electrons and holes for the 6 stable compounds and listed them in Table 1. The testified effective masses (m_e^* and m_h^*) of the carriers for CsPbBr₃ are 0.79 and 0.25 m_0 , which are slightly higher than the experimental measured 0.23 m_0 for both holes and electrons at room temperature.^[55] More often, the experimental measured physical parameters not only depend strongly on the crystal growth but also on other sample issues from the device fabrication.^[52,54,56] Thus, it is generally seen that the theoretic calculations can marginally deviate from the measured values. As shown in Table 1, the masses of holes in all Bi-based compounds are slightly heavier than the Sb-based compounds. This trend is in agreement with the weak coupling between the Bi(6s) and Sn(5s) orbitals, which results in narrow energy band dispersions at the valence band edges.^[17] Specifically, reducing the cation size from Rb⁺ to K⁺ makes the effective masses for electrons smaller while the holes become slightly heavier. This opposite carrier mass variation trend is in accord with the dispersion of band edges, which can be understood from the changing of hybridization between the orbital overlaps. For the larger bond angle distortions in K-based perovskites, the antibonding orbitals between X(p) with M(s) for the valence states are stabilized while the interactions with the M(p) orbitals for the conduction bands are destabilized, thereby reducing of band curvature in the valence edges but increasing it in the conduction band edges.^[3,53]

3.2.3. Optical Absorption Spectra

Figure 4 shows the calculated optical absorption spectra for the 6 stable $A_4MM'_2X_{12}$ by using PBE functional. It can be seen that these compounds exhibit strong absorption coefficient (above $5 \times 10^4 \text{ cm}^{-1}$) and steep absorption onset. A sharp absorption threshold is contributed by the dipole-allowed optical transitions with a high joint density of states (JDOS) near the band edges.^[57] From a qualitative viewpoint, the optical transitions from (Sn(s) + X(p)) to Sb/Bi(p) orbitals are dipole allowed and the relatively flat bands near the band edge guarantee a high JDOS, thereby resulting in an abrupt absorption onset.^[3,37,48]



Figure 4. a) Calculated spectrum of the optical absorption of the 6 stable $A_4MM'_2X_{12}$ compounds.

Though these ns^2 electronic compounds with high absorption coefficients and rapid onsets, the absorption spectra for Rb₄SnBi₂Cl₁₂ and K₄SnBi₂Cl₁₂ exist a slight reduction in the energy range of 3.3–3.7 eV. It implies a relatively weak hybridization of the subvalence bands in these Bi-based perovskites.

3.2.4. Electronic State Decorated by Different Orbital Hybridization

The density of states (DOS) calculations can accurately reproduce the discrete orbital contributions. In general, strong hybridization-induced broadening electronic states in solids requires both spatial and energy overlap between their orbital wavefunctions.^[2,3,58] Cations mixing breaks the translational and energetically connectivity of wavefunction to form discrete bands.^[58] As depicted by the red rectangle in **Figure 5a**, the conduction and valence band edges split into two separated peaks due to the incompatible orbital overlap between the Sn and Bi. From the atomic projected DOS, the conduction band edges in K₄SnBi₂Cl₁₂ are dominated from the weak hybridization between Bi(6p) and Sn(5p) orbitals with Cl(3p), while the valence band edges are contributed by the separated Sn²⁺ (5s²) and Bi³⁺ (6s²). We further schematically depicted these orbital coupling between the metal cation and halide ion near the band edges in **Figure 5b**. While for the projected DOS in Rb₄SnSb₂Br₁₂ (see in **Figure 5c,d**), the band edges state exhibit more dispersive contributions from both Sb and Sn, which implies a broadening of the orbital overlap between their 5s and 5p orbitals. One possible interpretation for the weak hybridization in Bi-based compounds is attributed to the contraction of Bi 6s and 6p orbitals by the relativistic effects, thus reducing the reactivity of shell electrons in comparison to the Sb-based compounds.^[17] Thus, the Sb-based perovskites show more broad orbital interactions for the band edges (see in **Figure 5c,d**).

3.3. Orbital Contributions to the Preferred $A_4MM'_2X_{12}$ Perovskites

The cubic ABX_3 perovskite structure is usually only observed at high temperature, while a group of lower symmetry phases emerges at lower temperatures.^[33] The associated new phases are driven by a range of symmetry breaking induced lattice tilting from the cubic phase.^[34,36] The relative stability of an inorganic halide perovskite tilting correlates with the volume decrease and the A-site displacement. For example, the prototypical halide perovskite CsSnBr₃ undergoes tilting phase transition sequence from high symmetry cubic α phase ($a^0a^0a^0$) to the low symmetry tetragonal β phase ($a^0a^0c^+$) and then to the orthorhombic γ phase ($a^-a^-c^+$) with gradually decreasing temperatures.^[36] As illustrated in **Figure 6**, two basic tilting modes induced phase transition accompanied octahedron rotation were denoted as M_3^+ and R_4^+ . The former is associated with the in-phase tilting of the octahedron in successive layers where every octahedron along the axis rotates in the same direction by the same amplitude, while the latter is corresponding to the out of phase tilting where the rotation changes sign for each octahedron along the rotation axis.^[35,36]

The layered $A_4MM'_2X_{12}$ perovskite is a B-site cation ordering structure which can be treated as a subgroup of the parent ABX_3 perovskites. Similar tilting modes can be used to enumerate the cation ordered layered structures, i.e., the M_3^+ and R_4^+ octahedral tilting mode in $A_4MM'_2X_{12}$ perovskites. However, it involves more complexity due to the layered charge ordering and its discontinuity along the [111] direction. In most cases, there exist tilting equivalents due to the cubic symmetry of the parent group, but the B-site cation order along the [111] direction makes the R_4^+ octahedral tilting to distinguishing between a positive ($a^-b^-c^0$) and a negative rotation ($-a^-b^-c^0$) along the [110] axis.^[34,35] The manifested octahedral tilting ($a^-b^-c^0$) in the relaxed Rb- and K-based $A_4MM'_2X_{12}$ perovskites begs further explaining of the physical origin of this tilting preference during the structure stabilization from the flat layered structures ($a^0b^0c^0$).

We illustrate the imposed electrostatic energy from the charge order coupling with the structure distortion by a simple model. As schematically shown in **Figure 7a**, the $\langle 111 \rangle$ -orientated tri-layered halide perovskite exhibits positive or negative net charges at each atomic plane, and the interfacial dipoles between them give rise to an internal electric field E .^[59,60] We employ a series of Gaussian surface between the polar atomic planes rising an alternative electric field profile (-2, +1, -1, +1, -1, +2) and finally become converged when across the 7 atomic planes due to the charge neutral of tri-layered perovskites. Thus, upon crossing the first negatively charged plane the potential gradient becomes negative (-2), and then become

reversed (+1) after crossing the second positively charged plane. Consequently, the electrostatic potential ϕ undergoes a dipole shift from the first atomic plane in combined with the symmetric oscillation component.^[60]

The octahedron tilting involves ion displacement from the flat atomic planes, thereby influencing electrostatic interactions from the charge redistribution.^[34,36] The R_4^+ octahedral tilting ($a^-b^-c^0$) has X^- ions departure from the $[AX_3]$

compared the relative energy in $\text{Rb}_4\text{SnSb}_2\text{Br}_{12}$ with different tilt modes, which shows consistent structural stability in the order of $-a^-b^-c^0 < a^0b^0c^0 < a^-b^-c^0 < a^-b^-c^+$.

Further evidence to support the above electrostatic analysis can be understood from the plane averaged electrostatic potential. As compared in Figure 7c, the intense oscillation of potential energy in the $\text{Rb}_4\text{SnSb}_2\text{Br}_{12}$ ($a^0b^0c^0$) become smoother in other three tilting structures due to the dipole reduction from the charged planes by ions intermixing. Particularly, in the $-a^-b^-c^0$ and $a^0b^0c^0$ tilting modes, the potential energy in the middle $[\text{RbBr}_3]^{2-}$ atomic planes are lower than that on the surface. This is consistent with a higher electron density at the middle atomic planes (see the black and blue arrows in

Sb(p)-Br(s/p) hybrid orbitals. Interestingly, the increased equatorial bonding intrigues the indirect-to-direct band transition due to the more upshift conduction band edge at G than Z point, see in Figure 8c. Note that the perovskites with indirect bandgap features are known to be beneficial for carrier recombination rates in optical absorbers, while the direct bandgaps would be a good attribute for light emission applications.^[2,61–63] Considering the strong direct gap optical transition and their bandgaps are in the visible light range (2.1–2.7 eV), the perovskites promise for high sensitivity detectors and efficient light-emitting diodes (LEDs) applications.^[64–66] The semiconductor detectors with large energy gaps (1.6–3.0 eV) can reduce the dark current noise from thermally activated carrier hopping.^[55] Additionally, the 2D layered structure in these perovskites provides a spatial limitation on the diffusion length of excitons and reduces the possibility of exciton dissociation into free carriers, and are, therefore, thought to be suitable for application as the light emissive layer in LEDs.^[64] These tilting modes couple with the electronic bands to give a versatile approach to tune the optoelectronic properties of the layered perovskites. To show the subtle variation, we plot the conduction band electron charge density contours at G (left) and Z (right) points under different tilting mode. As the electron charge density contour is shown in Figure 8d,e, the $a^-b^-c^0$ tilting mode exhibits more intense Sn(5p)-Br(4p)-Sb(5p) antibonding repulsion along the apical direction at Z point due to the in-plane bending of linear apical Sn-Br-Sb bonds. However, the $a^-b^-c^+$ tilting significantly diminishes the apical Sn-Br-Sb orbital interactions but intensify antibonding between the equatorial Sb(p)-Br(s/p)-Sn(p) hybrid orbitals extending in the y -direction at G point.

4. CONCLUSION

We take mixed cations of M^{2+} (Zn^{2+} and Sn^{2+}) plus M^{3+} (Bi^{3+} and Sb^{3+}) to explore the novel <111>-oriented tri-layered halide



- [40] G. Kresse, D. Joubert, *Ph. . Re. . B* **1999**, *59*, 1758.
- [41] J. Klimeš, D. R. Bowler, A. Michaelides, *J. Ph. .: Conden. . Ma. er* **2010**, *22*, 022201.
- [42] J. P. Perdew, K. Burke, M. Ernzerhof, *Ph. . Re. . Le. .* **1996**, *77*, 3865.
- [43] J. Heyd, G. E. Scuseria, M. Ernzerhof, *J. Chem. Ph. .* **2003**, *118*, 8207.
- [44] G. K. H. Madsen, D. J. Singh, *Comp. . Ph. . Comm. n.* **2006**, *175*, 67.
- [45] D. Yang, J. Lv, X. Zhao, Q. Xu, Y. Fu, Y. Zhan, A. Zunger, L. Zhang, *Chem. Ma. er.* **2017**, *29*, 524.
- [46] R. Fischer, B. G. Müller, *Z. Anorg. Allg. Chem.* **2002**, *628*, 1532.
- [47] S. W. Kim, R. Zhang, P. S. Halasyamani, M. A. Hayward, *Inorg. Chem.* **2015**, *54*, 6647.
- [48] M. H. Du, *J. Ma. er. Chem. C* **2014**, *2*, 4784.
- [49] Y. G. Yu, X. Zhang, A. Zunger, *Ph. . Re. . B* **2017**, *95*, 085201.
- [50] R. Gautier, X. Zhang, L. Hu, L. Yu, Y. Lin, T. O. L. Sunde, D. Chon, K. R. Poepplmeier, A. Zunger, *Na. . Chem.* **2015**, *7*, 308.
- [51] J. P. Perdew, A. Zunger, *Ph. . Re. . B* **1981**, *23*, 5048.
- [52] L. Pedesseau, J.-M. Jancu, A. Rolland, E. Deleporte, C. Katan, J. Even, *Op. . Q. an. m Elec. ron.* **2014**, *46*, 1225.
- [53] J. L. Knutson, J. D. Martin, D. B. Mitzi, *Inorg. Chem.* **2005**, *44*, 4699.
- [54] M. I. Dar, G. Jacopin, S. Meloni, A. Mattoni, N. Arora, A. Boziki, S. M. Zakeeruddin, U. Rothlisberger, M. Grätzel, *Sci. Ad. .* **2016**, *2*, e1601156.[545 [54]